



HAL
open science

Exceptional 20th century glaciological regime of a major SE Greenland outlet glacier

Camilla S. Andresen, Ulla Kokfelt, Marie-Alexandrine Sicre, Mads Faurschou Knudsen, Laurence M Dyke, Vincent Klein, Fanny Kaczmar, Martin W. Miles, David J. Wangner

► To cite this version:

Camilla S. Andresen, Ulla Kokfelt, Marie-Alexandrine Sicre, Mads Faurschou Knudsen, Laurence M Dyke, et al.. Exceptional 20th century glaciological regime of a major SE Greenland outlet glacier. Scientific Reports, 2017, 7, pp.13626. 10.1038/s41598-017-13246-x . hal-01629989

HAL Id: hal-01629989

<https://hal.sorbonne-universite.fr/hal-01629989>

Submitted on 7 Nov 2017

HAL is a multi-disciplinary open access archive for the deposit and dissemination of scientific research documents, whether they are published or not. The documents may come from teaching and research institutions in France or abroad, or from public or private research centers.

L'archive ouverte pluridisciplinaire **HAL**, est destinée au dépôt et à la diffusion de documents scientifiques de niveau recherche, publiés ou non, émanant des établissements d'enseignement et de recherche français ou étrangers, des laboratoires publics ou privés.



Distributed under a Creative Commons Attribution 4.0 International License

SCIENTIFIC REPORTS



OPEN

Exceptional 20th century glaciological regime of a major SE Greenland outlet glacier

Camilla S. Andresen¹, Ulla Kokfelt¹, Marie-Alexandrine Sicre², Mads Faurschou Knudsen³, Laurence M. Dyke¹, Vincent Klein², Fanny Kaczmar², Martin W. Miles^{4,5} & David Wangner¹

The early 2000s accelerated ice-mass loss from large outlet glaciers in W and SE Greenland has been linked to warming of the subpolar North Atlantic. To investigate the uniqueness of this event, we extend the record of glacier and ocean changes back 1700 years by analyzing a sediment core from Sermilik Fjord near Helheim Glacier in SE Greenland. We show that multidecadal to centennial increases in alkenone-inferred Atlantic Water SSTs on the shelf occurred at times of reduced solar activity during the Little Ice Age, when the subpolar gyre weakened and shifted westward promoted by atmospheric blocking events. Helheim Glacier responded to many of these episodes with increased calving, but despite earlier multidecadal warming episodes matching the 20th century high SSTs in magnitude, the glacier behaved differently during the 20th century. We suggest the presence of a floating ice tongue since at least 300 AD lasting until 1900 AD followed by elevated 20th century glacier calving due to the loss of the tongue. We attribute this regime shift to 20th century unprecedented low sea-ice occurrence in the East Greenland Current and conclude that properties of this current are important for the stability of the present ice tongues in NE Greenland.

In the last two decades there has been a rapid increase in the loss of ice from the Greenland Ice Sheet¹. A large part of this change has been attributed to increased iceberg calving from tidewater outlet glaciers^{2,3}, highlighting the role of marine-terminating glaciers in regulating ice-sheet stability. Mass change of the Greenland Ice-Sheet has only been continuously tracked with satellite data since the early 1990s. To understand whether the mass loss of the recent decade represents an outstanding event, or whether it is part of recurring phenomena acting on annual, decadal, or centennial timescales, we lack a longer-term history of the Greenland Ice Sheet. The answer to this question has potentially strong implications for the kind of ice-sheet changes we can expect in the context of future warming climate.

Concerns about glacier behavior emerged with the observation that many outlet glaciers on Greenland, including the three largest, suddenly increased their discharge at the turn of the 21st century⁴. Specifically Jakobshavn Isbræ, in West Greenland, and Kangerdlugssuaq and Helheim glaciers in SE Greenland (Fig. 1), accelerated, thinned, and retreated between 1996 and 2005^{1,4,5}. It was suggested that warming of subsurface ocean waters off West and SE Greenland triggered the acceleration and melting of these glaciers^{6–8}. The North Atlantic subpolar gyre (Fig. 1) delivers warm and salty subtropical waters to SE and West Greenland via the Irminger Current (IC). Saltier waters by Greenland have been observed in the mid- 1990s^{9,10} and attributed to a westward movement of the subpolar frontal system, which was caused by a weakening of the subpolar gyre circulation^{9,11}. As warm IC waters spread westward they penetrated further onto the SE and West Greenland continental shelf affecting the rate of submarine melting at glacier termini, thereby increasing iceberg calving rates and mass loss^{12,13}.

The link between climatic changes and outlet glacier variability during the past century has been demonstrated by a reconstruction of Helheim Glacier calving based on the combination of three sediment cores from Sermilik Fjord¹⁴. This high-resolution record (up to 1 year) documents several episodes of increased iceberg calving of which the youngest marked episode occurred between 2000 and 2005. This study found that regional

¹Geological Survey of Denmark and Greenland, Department of Glaciology and Climate, Øster Voldgade 10, 1350, Copenhagen K, Denmark. ²Sorbonne Universités (UPMC, Univ. Paris 06)-CNRS-IRD-MNHN, LOCEAN Laboratory, 4 place Jussieu, F-75005, Paris, France. ³Centre for Past Climate Studies, Department of Geoscience, Aarhus University, Høegh-Guldbergs Gade 2, 8000, Aarhus C, Denmark. ⁴Uni Research Climate / Bjerknes Centre for Climate Research, Bergen, Norway. ⁵Institute of Arctic and Alpine Research, University of Colorado, Boulder, CO, USA. Correspondence and requests for materials should be addressed to C.S.A. (email: csa@geus.dk)

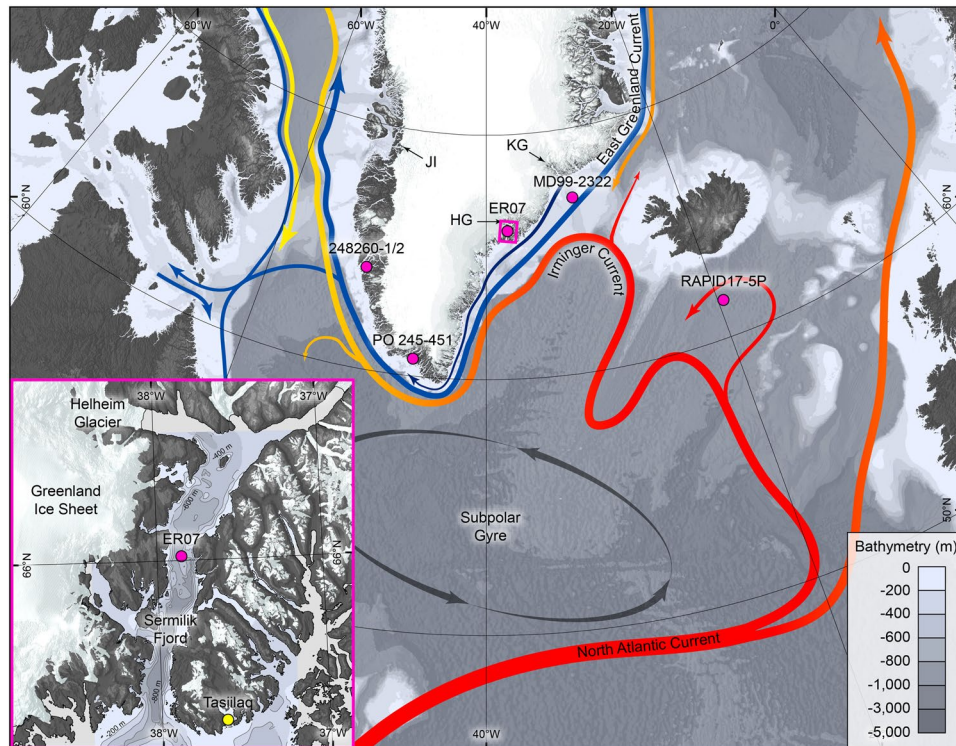


Figure 1. Map of the North Atlantic region showing the major surface ocean currents¹³ (colour of arrows indicate temperature; red = warm, blue = cold, yellow = mixture) and location of sites referred to in Fig. 3a–f. HG = Helheim Glacier; KG = Kangerdlugssuaq Glacier; JI = Jakobshavn Isbræ. Magenta circles show location of sediment cores discussed in the text and shown on Figs 2 and 3. The magenta box delineates the extent of the inset map. Bathymetric data are from IBCAO v3⁵⁶. Terrestrial topographic data are from the ETOPO1 Global Relief model⁵⁷ and the GIMP surface digital elevation model⁵⁸. The inset map of Sermilik Fjord shows the location of sediment core ER07 and the local bathymetry⁵⁹. The figure was created using ArcMap 10.1 (<http://desktop.arcgis.com/en/arcmap/>) and Adobe Illustrator CS6 (<http://www.adobe.com/products/illustrator.html>).

climatic modes (the North Atlantic Oscillation, NAO and the Atlantic Multidecadal Oscillation, AMO) may have influenced glacier calving through modulation of warm subsurface waters on the SE Greenland shelf and inside the fjord and that, conversely, episodes of increased cold polar waters occurrence may have potentially stabilised the glacier termini. However, almost nothing is known about the behaviour of Helheim Glacier before the 20th century and thus how on-going climate changes will affect the dynamics of outlet glaciers.

Here we extend the 20th century record of ocean and glacier variability back to 300 AD by analysing sediment core ER07 from Sermilik Fjord. Specifically, we use alkenone thermometry to reconstruct sea-surface temperature (SST). We assess the impacts of ocean conditions and sea-ice on the stability of Helheim Glacier using a reconstruction from the same core of iceberg sediment rafting while discussing the relationship between iceberg calving and sediment rafting. These new data provide the first-ever multi-centennial record of ocean and glacier changes that includes the 21st century changes in detail and thereby places the current changes into a longer temporal context embedding low frequency ocean variability.

Setting

Sermilik Fjord is situated in central SE Greenland; it is 80 km long, up to 15 km wide, and 600–900 m deep (Fig. 1). The two meter long sediment core ER07 was obtained from 525 m water depth (66°00′59″N, 37°51′07″W). Three outlet glaciers from the Greenland Ice Sheet drain into the north of the fjord; Helheim, Fenris, and Midgård Glaciers. Of these, Helheim Glacier is by far the largest and fastest and it is the third most prolific exporter of icebergs in Greenland². The ocean waters that circulate on the SE Greenland shelf dominate the subsurface waters in Sermilik Fjord. The hydrological vertical structure of the fjord is characterised by a 10–20 m thick surface layer of glacial melt water, a 100–150 m thick intermediate layer of cold Polar water, and a lowermost layer of warm saline water derived from the IC¹⁵. The primary driver for SST variability in coastal SE Greenland is the varying influence of the IC and the East Greenland Current (EGC), the two major currents that dominate the local hydrology^{14,16}.

Variability in sea surface temperature in SE Greenland shelf waters during the past 1700 years. Alkenone biomarkers, mainly produced by the coccolithophorid *Emiliana huxleyi*, have successfully been used for SST reconstructions in this region^{17,18}. This method was previously applied to core ER07 for reconstructing the SST variability of the last 100 years¹⁷. Our new 1700-year long record shows SSTs ranging from 6 to

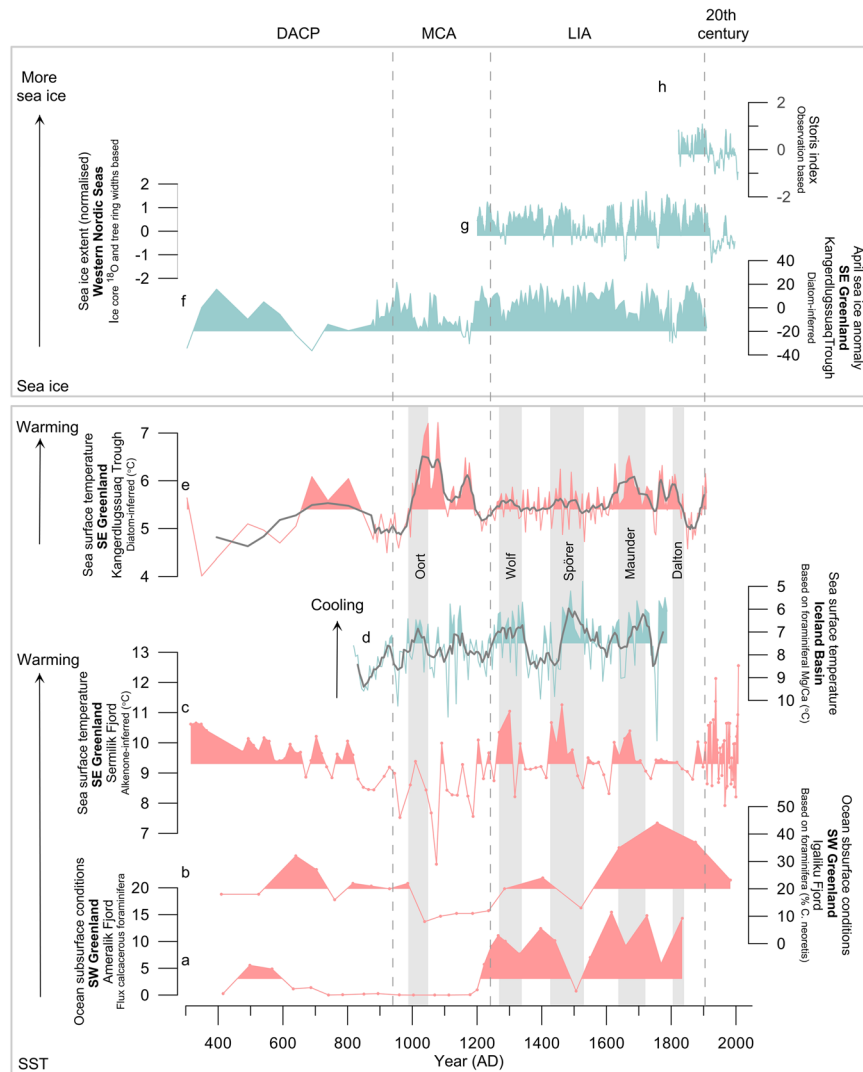


Figure 2. Paleoclimate records off and near Greenland. (a) Flux of calcareous foraminifera in core 248260–2 (Ameralik Fjord, SW Greenland) as indicator of subsurface ocean warming³⁹. (b) Relative amount (%) of foraminifera *C. neoteretis* in core PO 243–451 (Igaliku Fjord, SW Greenland) as indicator of ocean subsurface warming⁴⁰. (c) Alkenone-based SST reconstruction from sediment core ER07 (Sermilik Fjord, SE Greenland, this study). (d) Thermocline temperature reconstruction based in Mg/Ca in *G. inflata* from core RAPiD-17–5P plotted on a reversed Y axis (Iceland Basin)²⁸. (e) Diatom-based August SST reconstruction from core MD99–2322 (Kangerdlugssuaq Trough, SE Greenland)²⁶. (f) Diatom-based April sea-ice concentration anomalies in the same core as (e). (g) Greenland Sea winter sea-ice extent reconstruction of the Western Nordic Seas based on tree-ring widths and ice core ^{18}O records from Fennoscandia and Svalbard, respectively⁴³. (h) Fram Strait sea-ice export reconstruction from the Storö Index; a proxy for sea-ice in the EGC⁴⁶. Grey lines on (d) and (e) show 5-yr running means.

12.6°C (Fig. 2c), thus in a much larger range than the 0–4°C measured today in the surface waters in Sermilik Fjord¹⁶. This difference, already noticed in the previous study¹⁷, has been explained by the advection of allochthonous alkenones, i.e. not produced in Sermilik Fjord. Indeed, these authors have shown that alkenones found in Sermilik Fjord sediments are sourced from the high-productivity oceanic frontal region of the continental shelf outside the fjord, where present-day SSTs range from 8 to 13°C¹⁹ and advected into the fjord where they are deposited. Consequently, the alkenone-based temperature signal is indicative of the SST variability of the shelf waters entering the fjord¹⁷.

Our record shows multidecadal to centennial shifts in the temperature of surface ocean waters off SE Greenland with progressive cooling until the onset of the 20th century (Fig. 2c). The time series has been divided into four time periods on the basis of the centennial scale changes. The first period, from 300 AD to 950 AD, is characterised by high SSTs (mean 9.6°C), a long-term decrease and low variability (range 8.4–10.7°C). This period corresponds in Northwest Europe to the so-called Dark Ages Cold Period (DACP). The subsequent interval, between 950 AD and 1250 AD, contains among the lowest SSTs in the record (mean 8.5°C, range 6–10.1°C) progressively increasing from 6 to 10°C during the 11th and 12th centuries with a strong variability. This period

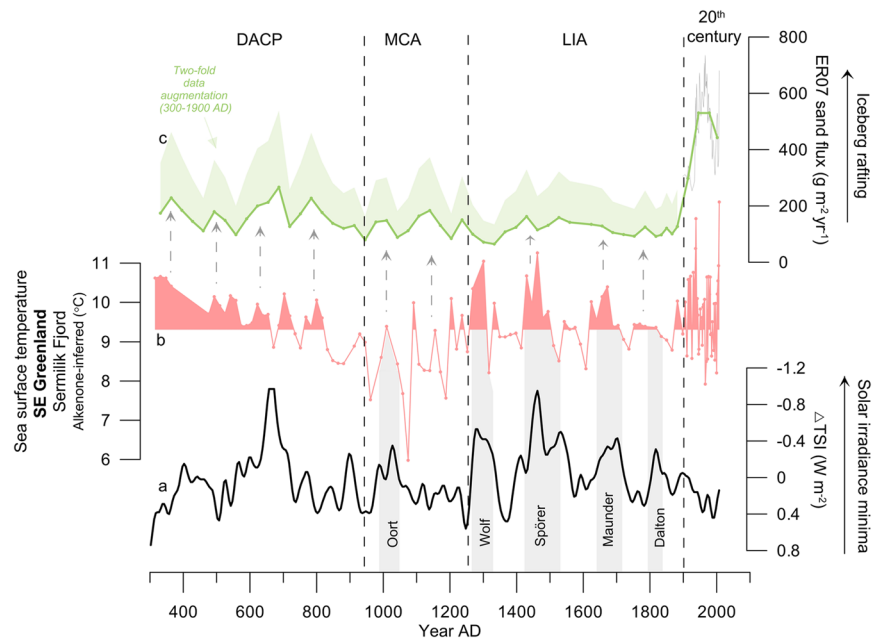


Figure 3. Core ER07 data from Sermilik Fjord and solar activity. **(a)** Solar irradiance reconstruction⁶⁰. **(b)** SST reconstruction from core ER07 in Sermilik Fjord, SE Greenland based on alkenone thermometry (this study). **(c)** Green line: sand flux in core ER07 used as a proxy for relative iceberg rafting (green shading: reconstruction augmented 300–1900 AD). In order to compare the lower and higher resolution portions of the IRD record, a 32 years binning was applied in data younger than 1900 AD (32 year is the average time resolution of samples older than 1900 AD). The original raw data are shown as a thin grey line. Grey stippled arrows indicate concurrent ER07 SST and ice rafting peaks. Grey bars indicate periods when increased SST concurs with low solar activity.

broadly coincides with the so-called Medieval Climate Anomaly (MCA), or Medieval Warm Period (MWP)²⁰ reported in numerous paleoclimate records though with different duration. Most MCA records, however, document warmer climatic conditions in the Northern Hemisphere, including near our study area in west and summit Greenland^{21,22} and off North Iceland²³ with concomitant low sea-ice cover²⁴.

The abrupt SST increase at the end of the 12th century marks the transition to a new temperature regime from 1250 AD to 1900 AD. This interval coincides with the Little Ice Age (LIA), a period of general atmospheric cooling and glacier advance in most sites of the Northern Hemisphere and expansion of sea-ice in the North Atlantic Ocean²⁵. The reconstructed SSTs during this interval are high (mean 9.4 °C; range 8.2–11.3 °C) and reveal a subtle cooling trend and greater variability than during the DACP. Three notable warm periods are salient around 1270–1300 AD, 1430–1460 AD, and 1620–1670 AD.

From the early 20th century to present-day, average SSTs increased slightly (mean 9.8 °C, range 7.9–12.6 °C) to values that are comparable to the mean conditions during earlier warm episodes of both the DACP and the LIA. The higher variability of SSTs during the 20th century could in part be due to the higher temporal resolution of the record in this interval (Fig. 2c).

Due to the scarcity of dateable material in glacioproximal sediments¹⁴C dating constraints before 1900 AD are sparse in core ER07 (Supplementary Table S1). To increase robustness in our age model in the interval 300–1900 AD we compared the Sermilik SST record with the more densely dated SST record from nearby Kangerdlugssuaq Trough core MD99–2322²⁶, established from four ¹⁴C dates and one tephra layer (Fig. 1 and Fig. 2e). In similarity with the continental shelf offshore Sermilik Fjord, the Kangerdlugssuaq Trough warm waters originate from the Irminger Sea via the IC¹³. Therefore, it is expected that multidecadal ocean variability in the Irminger Sea and IC would be reflected in both SST records. The EGC is also expected to influence SSTs similarly at the two sites, although the generally higher sea-ice occurrence by the more northerly Kangerdlugssuaq Trough may explain differences in absolute SST values at the two sites. Comparison of the multidecadal SST variability in both records shows a highly significant positive correlation for the period after the MCA (1230–1900 AD) ($R = 0.29$; $P = 0.03$) when compared to randomly generated red-noise data, and a positive correlation for the period 300–900 AD ($R = 0.42$; $P = 0.12$), although only marginally significant, which is probably due to the low data-resolution in core MD99–2322 (see supplementary information for statistical analysis). These results strengthen our confidence in the age model for core ER07.

Drivers of ocean variability off SE Greenland. The comparison of our new SST record with a reconstruction of past changes in total solar irradiance (TSI) (Fig. 3a,b) indicates that episodes of warmer SSTs occurred during periods of low solar activity. It is particularly striking that SST maxima are largely concurrent with the well-known Wolf, Spörer, Maunder and Dalton solar minima of the LIA. This visual match is underpinned by a highly significant negative correlation ($R = -0.43$; $P = 0.02$) between the TSI and our new SST record from

Sermilik Fjord across the four solar minima that followed the MCA (1230–2000 AD). This relationship is further supported by wavelet analyses showing high common power in both records at periodicities between 120–210 years, and significant wavelet coherence at these periodicities, between 1230 and 1800 AD (Supplementary Figs S1 and 2).

Links between changes in solar activity and oceanic conditions around Greenland and the North Atlantic Ocean have previously been demonstrated^{26–29}. The physical mechanisms at play remain debated³⁰, but considering the small amplitude of the variations in TSI, amplifying mechanisms are likely to explain the magnitude of climate variability in paleo-records. Climate modelling has demonstrated that atmospheric circulation responds to low solar activity by resembling the negative phase of the winter NAO^{31,32}. Other modeling studies have shown that solar minima of the 20th century and the Maunder Minimum favor persistent North Atlantic anticyclonic blocking³³. This weather regime has been related to the negative phase of the East Atlantic pattern (EA⁻) and shown to be responsible for the most severe winters on record in Europe³⁴. This mode of variability has a similar North South dipole structure as the NAO but its centers of action are displaced southeastward. Both NAO and EA are important drivers of the North Atlantic Ocean circulation. The response of the ocean to weaker westerly winds (negative NAO) as well as persistent blocking events across the Atlantic is a wind-driven reduction and shrinking of the subpolar gyre^{9,35,36}. Indeed, oceanic warming in West Greenland at the turn of the 21st century has been paralleled to a decrease from high positive NAO index values in the early 1990s to negative state in 1996 and the strong decline of the subpolar gyre circulation⁹. In a recent study, the role of negative EA and blocked events on the subpolar gyre circulation has been evidenced³⁵. Therefore, negative NAO and persistent blocking events favored by reduced solar activity are likely to explain the warm oscillations of the Atlantic waters seen off SE Greenland (Sermilik and Kangerdlugssuaq²⁹) and the generally higher temperatures during the LIA than MCA off Sermilik Fjord. In contrast to SE Greenland, in the RAPID17–5P core south of Iceland, solar activity positively correlates with SSTs²⁸ (Fig. 2d). This response to TSI changes is in accordance with a negative correlation between SST variations south of Iceland and offshore Sermilik Fjord ($R = -0.26$; $P = 0.05$) (see supplementary information). This finding underlines contrasting oceanic conditions between the SPG and the colder and fresher NAC⁹ as a result of the extension and shape of the SPG and subsequent position of the NAC, although more recent studies have shown that the eastern and western branch of the subpolar gyre may respond differently to atmospheric forcings^{36,37}. Our record shows that both DACP and the LIA were characterised by high SSTs near Sermilik Fjord (Fig. 2c). Warming of sub-surface IC-sourced waters during the DACP and LIA has been reported at other sites on the Southern Greenland shelf^{38–40} (Fig. 2a,b) suggesting that warmer and/or higher proportion of warm IC-sourced waters spilled onto the Greenland shelf. Indeed, temperature of the Greenland shelf is a function of both upstream NAC water temperature and the subpolar gyre strength. While high shelf SSTs during the LIA was linked with centennial scale weakening of the subpolar gyre induced by low solar activity, this may not have necessarily been the case during the DACP.

The intervening MCA period from 950 to 1250 AD of generally cold SSTs near SE Greenland (Fig. 2c) was characterized by a lesser influence of IC-sourced subsurface waters on the southern Greenland shelf^{38–40} (Fig. 2a,b). This is in contrast with the generally warmer SSTs of the NAC due to increased northwards heat transport under stronger Westerlies that presumably prevailed during the MCA⁴¹. Therefore, cooling of the Greenland shelf waters indicates that stronger westerlies while expanding eastwards and strengthening the subpolar gyre would have diminished the inflow of IC-sourced waters onto the Greenland shelf. The generally lower sea-ice occurrence in the EGC during the MCA is reflected in the overall higher SST values, as for example, north of our core site, by Kangerdlugssuaq Trough²⁶ (Figs 1 and 2e). SSTs at this location were modulated to a greater extent by sea-ice occurrence in the EGC with warm MCA being a period of broadly reduced sea-ice^{26,42} (Fig. 2f–h) as also observed off North Iceland²⁴.

According to the new data from SE Greenland core ER07 presented here, the average 20th century SSTs of IC-sourced waters off Greenland was high, but not any higher than during the earlier multidecadal episodes of warming. At the same time sea-ice occurrence in the EGC during most of the 20th century was unprecedentedly low^{43–46} (Fig. 2g,h).

20th and 21st century mass loss from Helheim Glacier in a 1700 year context. To investigate the response of Helheim glacier over the past 1700 years of ocean changes near Sermilik Fjord the relative variability in glacier melt and iceberg production is assessed. This is done by reconstructing the relative variability in the amount of sediment-laden icebergs exiting the fjord. A high-resolution calculation of the sand flux (i.e. the amount of sand deposited per area sea-bed per year; Supplementary Fig. S3) in the sediment core (Fig. 3c) is generated, relying on the assumption that sand grains are too large to be advected in the meltwater plume, and consequently must have been rafted into the fjord by icebergs. This method was applied in a previous study combining three sediment cores from Sermilik fjord (including ER07)¹⁴ (Supplementary Figs S3 and S4) and demonstrated the applicability of ice rafted debris (IRD) in Sermilik Fjord as a proxy for iceberg production (calving) from Helheim Glacier.

The 1700-year long record from Sermilik Fjord reveals a decrease in iceberg rafting from 300 AD to 1300 AD (Fig. 3c). This is followed by a period of stabilized iceberg debris accumulation that terminates with a marked increase at around 1900 AD; this final phase persisted through the 20th century to the present. A pronounced increase in sedimentation rate during the 20th century is also found in a more southerly core from Sermilik Fjord (Supplementary Figs S4 and S5). Multidecadal variability prevails in the ER07 ice rafting signal and many of the relatively short-lived ice rafting episodes coincide with short-lived SST peaks (Fig. 3c). Near-synchronous pattern of calving in Sermilik Fjord, negative NAO index, and warming of the IC near Greenland was evidenced during the 20th century¹⁴. Based on comparison to red-noise data, however, a statistically significant relationship between ice-rafting episodes and SST variations cannot be recognised for the entire period prior to the 20th century (see supplementary information). We suggest that those of the pre-20th century multidecadal ice rafting episodes that

are concurrent with increased SSTs relate to climatically forced increased iceberg calving. This indicates that some ice rafting events may be related to intrinsic glacier behavior and that some of the IC warming episodes did not result in glaciological changes.

The cause of unprecedented levels of iceberg rafting throughout the 20th century is unexpected since average SSTs during the 20th century were similar to those during previous multidecadal warming episodes. We suggest that the unprecedented high iceberg rafting from Helheim Glacier after 1900 AD links with unprecedented reductions in sea-ice in the EGC after 1900 AD (Fig. 2g,h). The lowered sea-ice abundance in the EGC during the 20th century may have increased air temperatures markedly in coastal areas of SE Greenland after 1900 AD, as supported by lake sediment studies nearby Sermilik Fjord designating the 20th century warming as a conspicuous feature over several millennia^{47,48}.

Thus the higher sea-ice abundance in the EGC and relatively low air temperatures in coastal areas of SE Greenland prior to the early 1900s, may have suppressed iceberg calving in addition to depriving icebergs of sediment; together resulting in low levels of iceberg rafting during this interval. Modern observations demonstrate that air cooling and attendant decrease in meltwater production can inhibit glacier discharge; this occurs through a reduction in hydrofracturing of crevasses⁴⁹ and an increase in basal friction⁵⁰. Lower air temperatures may also increase the rigidity of the mélange of icebergs in front of Helheim glacier⁵¹. This would serve to stabilise the glacier margin and decrease calving during cold climatic conditions. However, the relatively limited trimlines around the terminus of Helheim Glacier indicates that its mass loss since the LIA has been relatively low, especially when compared with the large post-LIA mass loss from Jakobshavn Isbræ and Kangerdlugssuaq Glacier⁵². This observation indicates that the nearly four-fold increase in iceberg rafting in Sermilik Fjord after the LIA may not be explained exclusively by increased iceberg calving. We therefore suggest that Helheim Glacier may have developed a floating ice tongue in response to increases in sea-ice and cold atmospheric conditions between 300 AD and the early 1900s. Under this scenario melt-out of debris-rich basal ice from the glacier margin would be expected to increase resulting in a reduction in iceberg sediment content. Finally, if cold coastal air temperatures prior to the early 1900s increased the cohesiveness of the glacial mélange and resulted in local enhanced sea-ice cover beyond the mélange, this would increase iceberg residence times in the upper-fjord. Increased residence time of icebergs may result in enhanced melt-out of debris before icebergs transit the core site and thereby decrease iceberg rafting.

The reconstruction of iceberg rafting from Helheim Glacier together with SSTs of the shelf waters allows us to set recent dramatic glacier changes in SE Greenland into a longer-term context. It was recently found that the 2000–2005 AD increase in glacier calving may have been matched in magnitude by a similar event in the 1930s¹⁴. However, the current study indicates that elevated levels of iceberg calving during the 20th century were unprecedented in the last 1700 years. Moreover, our new record shows that the high 20th century SSTs were matched during several previous multidecadal warm episodes during the DACP and LIA, yet the IRD record demonstrates that Helheim Glacier behaved differently in the 20th century. We attribute this finding to the presence of a relatively marked floating tongue at Helheim Glacier at least since the DACP, lasting until the abrupt end of the LIA in the early 20th century and suggest that the glaciological regime shift was triggered by unprecedented low sea-ice concentrations in the EGC during the 20th century. Part of the mass loss before the 20th century would have taken place via submarine melt underneath this floating tongue, similar to the mass loss from more northerly ice streams of the Greenland Ice Sheet, such as Nioghalvfjærdsbræ Glacier⁵³. Our results imply that model predictions of dynamic loss from ice streams in North Greenland need to account for threshold effects from sea-ice to better predict the future evolution of Greenland coastal glaciers in a warming North Atlantic Ocean.

Material and Methods

Sediment core ER07 was obtained using a Rumohr corer, using 80 mm core liner, from 525 m water depth (66°00'59"N, 37°51'07"W). X-ray imagery¹⁴ (Supplementary Fig. S6) shows that the core consists of massive diamicton facies with abundant pebbles. A very sandy unit occurs below an erosional boundary at 124 cm. The upper-124 cm represents the last 1700 years of sedimentation, whereas a single radiocarbon date indicates an age of the sediment below the erosional boundary of ~8800 cal. yrs BP (Supplementary Table S1). The chronology of core ER07 was constructed by combining a ²¹⁰Pb model of the upper 25.5 cm¹⁴ (Supplementary Table S2) with the radiocarbon date from level 120 cm in the core (Supplementary Fig. S6, Supplementary Table S1) using linear interpolation. The temporal resolution ranges from 1 to 4 years in the interval dated by ²¹⁰Pb, and on average 16 years in the lower portion of the core constrained by ¹⁴C dating. The associated sedimentation rate for the same periods (before and after AD 1900) is 0.06 cm yr⁻¹ and 0.13–0.5 cm yr⁻¹ (average 0.25 cm yr⁻¹), respectively. Material for grain size analysis was continuously sampled at intervals of 0.5 cm down to 26 cm, at 1 cm intervals between 26 and 31 cm, and at 2 cm intervals below 31 cm. The grain size distribution (volume %) was estimated by a Malvern Mastersizer 2000 laser particle sizer. Samples were dispersed with sodium pyrophosphate (0.01 M Na₄P₂O₇ × 10 H₂O) and treated in an ultrasound bath for two minutes before measuring the 0.3–1000 µm fraction. The flux of sand (>63 µm) was calculated as a function of the wt % of sand, sedimentation rate and dry bulk density.

Alkenones comprise a suite of methyl and ethyl C₃₇ to C₃₉ ketones with two or three double bonds that are produced primarily by the ubiquitous marine coccolithophorides *Emilinia huxleyi*. SSTs were obtained from the unsaturation ratio of C₃₇ alkenones ($U_{37}^K = C_{37:2}/(C_{37:2} + C_{37:3})$) and the global calibration ($T = (U_{37}^K - 0.039)/0.034$)⁵⁴, a well-established temperature proxy in paleoceanographic studies. Precision based on triplicate injections on selected samples has been estimated to be 0.3°C. The SST reconstruction was built from the downcore U_{37}^K values acquired at a sample step of 1 cm. Biomarkers were extracted from 5 gr of freeze-dried sediments with a mixture of methanol/methylene chloride (1:2 v/v). Alkenones were isolated from the total lipid extract by open column silica gel chromatography using solvent mixtures of increasing polarity. Gas chromatography analyses were performed to achieve individual alkenone separation and subsequent quantification. Details on the analytical procedure can be found in ref.⁵⁵. The recent 100 years of the grain size and alkenone data were published in refs.^{14,17}.

Binning of IRD data younger than 1900 was done by calculating the average sand flux in the following time intervals 1898–1930, 1931–1962, 1963–1996, 1997–2008 (AD).

References

- Rignot, E., Velicogna, I., van den Broeke, M. R., Monaghan, A. & Lenaerts, J. T. M. Acceleration of the contribution of the Greenland and Antarctic ice sheets to sea level rise. *Geophysical Research Letters* **38**, L05503, <https://doi.org/10.1029/2011GL046583> (2011).
- Rignot, E. & Kanagaratnam, P. Changes in the velocity structure of the Greenland Ice Sheet. *Science* **311**, 986–990, <https://doi.org/10.1126/science.1121381> (2006).
- Van den Broeke, M. *et al.* Partitioning recent Greenland mass loss. *Science* **326**, 984–986, <https://doi.org/10.1126/science.1178176> (2009).
- Howat, I. M., Joughin, I. & Scambos, T. E. Rapid changes in ice discharge from Greenland outlet glaciers. *Science* **315**, 1559–1561, <https://doi.org/10.1126/science.1138478> (2007).
- Thomas, R. H. *et al.* Investigation of surface melting and dynamic thinning on Jakobshavn Isbrae. *Journal of Glaciology* **49**, 231–239, <https://doi.org/10.3189/172756503781830764> (2003).
- Holland, D. M., Thomas, R. H., De Young, B., Ribergaard, M. H. & Lyberth, B. Acceleration of Jakobshavn Isbræ triggered by warm subsurface ocean waters. *Nature Geoscience* **1**, 659–664, <https://doi.org/10.1038/ngeo316> (2008).
- Straneo, F. *et al.* Characteristics of ocean waters reaching Greenland's glaciers. *Annals of Glaciology* **53**, 202–210 (2012).
- Murray, T. *et al.* Ocean regulation hypothesis for glacier dynamics in SE Greenland and implications for ice sheet mass changes. *J. Geophys. Res.* **115**, F03026, <https://doi.org/10.1029/2009JF001522> (2010).
- Hatun, H., Sandø, A. B., Drange, H., Hansen, B. & Valdimarsson, H. Influence of the Atlantic Subpolar gyre on the thermohaline circulation. *Science* **309**, 1841–1844 (2005).
- Stein, M. North Atlantic Subpolar gyre warming – impacts on Greenland offshore waters. *Journal of Northwest Atlantic Fishery Science* **36**, 43–54 (2005).
- Häkkinen, S. & Rhines, P. B. Decline of subpolar North Atlantic Circulation during the 1990s. *Science* **304**, 555–559 (2004).
- Rignot, E., Koppes, M. & Velicogna, I. Rapid submarine melting of the calving faces of West Greenland glaciers. *Nature Geoscience* **3**, 187–191 (2010).
- Straneo, F. & Heimbach, P. North Atlantic warming and the retreat of Greenland's outlet glaciers. *Nature* **504**, 36–43 (2013).
- Andresen, C. S. *et al.* Rapid response of Helheim Glacier in Greenland to climate variability over the past century. *Nature Geoscience* **5**, 37–41 (2012).
- Straneo, F. *et al.* Impact of fjord circulation and glacial runoff on the circulation near Helheim Glacier. *Nature Geoscience* **4**, 322–327 (2011).
- Straneo, F. *et al.* Rapid circulation of warm subtropical waters in a major glacial fjord in East Greenland. *Nature Geoscience* **3**, 182–186 (2010).
- Andresen, C. S. *et al.* A 100-year long record of alkenone-derived SST changes by SE Greenland. *Continental Shelf Research* **71**, 45–51 (2013b).
- Sicre, M.-A. *et al.* Labrador current variability over the last 2000 years. *Earth and Planetary Science Letters* **400**, 26–32 (2014).
- Sutherland, D. F. *et al.* Atlantic water variability on the SE Greenland continental shelf and its relationship to SST. *Journal of Geophysical Research: Oceans* **118**, 1–9, <https://doi.org/10.1029/2012JC008354> (2013).
- Lamb, H. H. The early medieval warm epoch and its sequel. *Palaeogeography, Palaeoclimatology, Palaeoecol.* **1**, 13–37 (1965).
- D'Andrea, W. J., Huang, Y., Fritz, S. C. & Anderson, N. J. Abrupt Holocene climate change as an important factor for human migration in West Greenland. *Proceedings of the National Academy of Sciences* **108**, 9765–9769 (2011).
- Dahl-Jensen, D. *et al.* Past temperatures directly from the Greenland ice sheet. *Science* **282**, 268–271 (1998).
- Sicre, M.-A. *et al.* Decadal variability of sea surface temperatures off North Iceland over the last 2000 years. *Earth and Planetary Science Letters* **268**, 137–142 (2008).
- Massé, G. *et al.* Abrupt climate changes for Iceland during the last millennium: Evidence from high resolution sea-ice reconstructions. *Earth and Planetary Science Letters* **3–4**, 565–569 (2008).
- Grove, J. M. The initiation of the “Little Ice Age” in regions around the North Atlantic. *Climatic Change* **48**, 53–82 (2001).
- Miettinen, A., Divine, D. V., Husum, K., Koç, N. & Jennings, A. Exceptional ocean surface conditions on the SE Greenland shelf during the Medieval Climate Anomaly. *Paleoceanography* **30**, 1–17 (2015).
- Sejrup, H. P. *et al.* Response of Norwegian sea temperature to solar forcing since 1000 AD. *J. Geophysical Res.* **115**, C12034 (2010).
- Moffa-Sanchez, P., Born, A., Hall, I. R., Thornalley, J. R. & Barker, S. Solar forcing of North Atlantic surface temperature and salinity over the past millennium. *Nature Geoscience* **7**, 275–278 (2014).
- Sha, L. *et al.* Solar forcing as an important trigger for West Greenland sea-ice variability over the last millennium. *Quaternary Science Reviews* **131**, 148–156 (2016).
- Gray, L. J. *et al.* Solar influences on climate. *Review of Geophysics* **48**, RG4001, <https://doi.org/10.1029/1009RG000282> (2010).
- Schindell, D. T., Schmidt, G. A., Mann, M. E., Rind, D. & Waple, A. Climate changes during the Maunder Minimum. *Science* **294**, 2149–2152 (2001).
- Raible, C. C., Yoshimori, M., Stocker, T. & Casty, C. Extreme midlatitude cyclones and their implications for precipitation and wind speed extremes in simulations of the Maunder Minimum versus present day conditions. *Climate Dynamics* **28**, 409–423, <https://doi.org/10.1007/s00382-006-0188-7> (2007).
- Barrripedro, D., Garcia-Herrera, R. & Huth, R. Solar modulation of Northern Hemisphere winter blocking. *J. Geophys. Res., Atmos.* **113**, D14118, <https://doi.org/10.1029/2008JD009789> (2008).
- Moore, G. W. K. & Renfrew, I. A. Cold European winters: interplay between the NAO and the East Atlantic mode. *Atmospheric Science Letters* **13**, 1–8 (2012).
- Häkkinen, S., Rhines, P. B. & Worthen, D. L. Atmospheric blocking and Atlantic multidecadal ocean variability. *Science* **334**, 656569 (2011).
- Barrier, N., Cassou, C., Deshayes, J. & Treguier, A.-M. Response of North Atlantic Ocean circulation to atmospheric weather regimes. *Journal of Physical Oceanography* **44**, 179–201, <https://doi.org/10.1175/JPO-D-12-0217.1> (2014).
- Barrier, N., Deshayes, J. & Treguier, A.-M. & Cassou, C. Heat budget in the North Atlantic Subpolar Gyre: Impacts of atmospheric weather regimes on the 1995 warming event. *Progress in Oceanography* **130**, 75–90, <https://doi.org/10.1016/j.pocean.2014.10.001> (2015).
- Andresen, C. S. *et al.* Mid- to late-Holocene oceanographic variability on the SE Greenland shelf. *The Holocene* **23**, 167–178 (2013a).
- Seidenkrantz, M.-S. *et al.* Hydrography and climatic change during the last 4.400 years in Ameralik Fjord, SW Greenland. *The Holocene* **17**(3), 387–401 (2007).
- Lassen, S. *et al.* Late-Holocene Atlantic bottom-water variability in Igaliku Fjord, South Greenland, reconstructed from foraminifera faunas. *The Holocene* **14**(2), 165–171 (2004).
- Trouet, V. *et al.* Persistent positive North Atlantic Oscillation mode dominated by the Medieval Climate Anomaly. *Science* **324**, 78–80 (2009).
- Jennings, A., Andrews, J. & Wilson, L. Holocene environmental evolution of the SE Greenland Shelf North and South of the Denmark Strait: Irminger and EGC interactions. *Quaternary Science Reviews* **30**, 980–998 (2011).
- Macias Fauria, M. *et al.* Unprecedented low twentieth century winter sea-ice extent in the Western Nordic seas since A.D. 1200. *Climate Dynamics* **34**, 781–795 (2010).
- Cabedo-Sanz, P. & Belt, S. Seasonal sea-ice variability in eastern Fram Strait over the last 2000 years. *Arktos* **2**, 22, <https://doi.org/10.1007/s41063-016-0023-2> (2016).

45. Perner, K., Moros, M., Lloyd, J. M., Jansen, E. & Stein, R. Mid to late Holocene strengthening of the EGC linked to warm subsurface Atlantic water. *Quaternary Science Reviews* **129**, 296–307 (2015).
46. Schmith, T. & Hansen, C. Fram Strait ice export during the nineteenth and twentieth centuries reconstructed from a multiyear sea-ice index from southwestern Greenland. *Journal of Climate* **16**, 2782–2791 (2003).
47. Balascio, N. L., D'Andrea, W. J., Bradley, R. S. & Perren, B. B. Biogeochemical evidence for hydrologic changes during the Holocene in a lake sediment record from southeast Greenland. *The Holocene* **23**(10), 1428–1439, <https://doi.org/10.1177/0959683613493938> (2013).
48. Jakobsen, B. H., Fredskild, B. & Pedersen, J. B. T. Holocene changes in climate and vegetation in the Ammassalik area, East Greenland, recorded in lake sediments and soil profiles. *Danish Journal of Geography* **108**(1), 21–50 (2008).
49. Foga, S., Stearns, L. A. & van der Veen, C. J. Application of satellite remote sensing techniques to quantify terminus and ice mélange behavior at Helheim Glacier, SE Greenland. *Marine Technology Society Journal* **48**(5), 81–91, <https://doi.org/10.4031/MTSJ.48.5.3> (2014).
50. Everett, A. *et al.* Annual down-glacier drainage of lakes and water-filled crevasses at Helheim Glacier, SE Greenland. *Journal of Geophysical Research: Earth Surface* **121**, 1819–1833 (2016).
51. Amundsson, J. M. *et al.* Ice mélange dynamics and implications for terminus stability, Jakobshavn Isbræ, Greenland. *Journal of Geophysical Research* **115**, F01005, <https://doi.org/10.1029/2009JF001405> (2010).
52. Kjeldsen, K. K. *et al.* Spatial and temporal distribution of mass loss from the Greenland ice sheet since AD 1900. *Nature* **528**, 396–400 (2015).
53. Khan, S. A. *et al.* Sustained mass loss of the northeast Greenland ice sheet triggered by regional warming. *Nature Climate Change* **4**, 292–299 (2014).
54. Prah, F. G., Muehlhausen, L. A. & Zahnle, D. L. Further evaluation of long-chain alkenones as indicators of paleoceanographic conditions. *Geochimica et Cosmochimica Acta* **52**, 2302–2310 (1988).
55. Ternois, Y., Sicre, M.-A., Boireau, A., Marty, J.-M. & Miquel, J.-C. Production pattern of alkenones in the Mediterranean Sea. *Geophysical Research Letters* **23**, 3171–3174 (1996).
56. Jakobsson, M. *et al.* The International Bathymetric Chart of the Arctic Ocean (IBCAO) Version 3.0. *Geophysical Research Letters* **39**, L12609, <https://doi.org/10.1029/2012GL052219> (2012).
57. Amante, C. & Eakins, B. W. ETOPO1 1 Arc-Minute Global Relief Model: Procedures, Data Sources and Analysis. NOAA Technical Memorandum NESDIS NGDC-24, National Geophysical Data Center, NOAA (2009).
58. Howat, I. M., Negrete, A. & Smith, B. E. The Greenland Ice Mapping Project (GIMP) land classification and surface elevation datasets. *The Cryosphere* **8**, 1509–1518 (2014).
59. Schjøth, F. *et al.* Campaign to Map the Bathymetry of a Major Greenland Fjord. *EOS, Transactions American Geophysical Union* **93**, 141–142 (2012).
60. Steinhilber, F., Beer, J. & Fröhlich, C. Total solar irradiance during the Holocene. *Geophysical Research Letters* **36**, L19704, [doi:10.1029/2009GL04142](https://doi.org/10.1029/2009GL04142) (2009).

Acknowledgements

We gratefully acknowledge funding for this study from the VILLUM Foundation to the project ‘Past and future dynamics of the Greenland Ice Sheet: what is the ocean hiding?’ (grant no. 10100). We thank the Centre National de la Recherche Scientifique (CNRS) for salary support. We also acknowledge support from the ice2ice project funded by the European Research Council (ERC grant no. 610055), the Norwegian Research Council, and the Centre for Climate Dynamics at the Bjerknes Centre. We thank R. Fausto, A. Solgaard, T. Cronin and the Ocean2k working group of the Past Global Changes (PAGES) for discussions and three anonymous reviewers for help in improving the manuscript.

Author Contributions

C.S.A. conceived the study and undertook fieldwork. C.S.A., U.K. and M.A.S. wrote most of the initial manuscript. M.F.K. conducted statistical analysis. V.K. and F.K. conducted alkenone analysis. M.F.K., L.M.D., M.W.M. and D.J.W. contributed to the writing of the manuscript.

Additional Information

Supplementary information accompanies this paper at <https://doi.org/10.1038/s41598-017-13246-x>.

Competing Interests: The authors declare that they have no competing interests.

Publisher's note: Springer Nature remains neutral with regard to jurisdictional claims in published maps and institutional affiliations.



Open Access This article is licensed under a Creative Commons Attribution 4.0 International License, which permits use, sharing, adaptation, distribution and reproduction in any medium or format, as long as you give appropriate credit to the original author(s) and the source, provide a link to the Creative Commons license, and indicate if changes were made. The images or other third party material in this article are included in the article's Creative Commons license, unless indicated otherwise in a credit line to the material. If material is not included in the article's Creative Commons license and your intended use is not permitted by statutory regulation or exceeds the permitted use, you will need to obtain permission directly from the copyright holder. To view a copy of this license, visit <http://creativecommons.org/licenses/by/4.0/>.

© The Author(s) 2017